RESEARCH ARTICLE

Key Points:
- More upstream PCWs at Venus near solar maximum compared to solar minimum
- Increase due to higher ratio of planetary to SW proton density
- Asymmetry in IMF at PCWs due to tilt of heliospheric current sheet

Correspondence to:
M. Delva,
magda.delva@oeaw.ac.at

Upstream proton cyclotron waves at Venus near solar maximum

M. Delva[1], C. Bertucci[2], M. Volwerk[1], R. Lundin[3], C. Mazelle[4], and N. Romanelli[2]

[1]Space Research Institute, Austrian Academy of Sciences, Graz, Austria, [2]Institute for Astronomy and Space Physics, Buenos Aires, Argentina, [3]Swedish Institute for Space Physics, Kiruna, Sweden, [4]IRAP UPS-CNRS, Toulouse, France

Abstract Long-term magnetometer data of Venus Express are analyzed for the occurrence of waves at the proton cyclotron frequency in the spacecraft frame in the upstream region of Venus, for conditions of rising solar activity. The data of two Venus years up to the time of highest sunspot number so far (1 Mar 2011 to 31 May 2012) are studied to reveal the properties of the waves and the interplanetary magnetic field (IMF) conditions under which they are observed. In general, waves generated by newborn protons from exospheric hydrogen are observed under quasi- (anti)parallel conditions of the IMF and the solar wind velocity, as is expected from theoretical models. The present study near solar maximum finds significantly more waves than a previous study for solar minimum, with an asymmetry in the wave occurrence, i.e., mainly under antiparallel conditions. The plasma data from the Analyzer of Space Plasmas and Energetic Atoms instrument aboard Venus Express enable analysis of the background solar wind conditions. The prevalence of waves for IMF in direction toward the Sun is related to the stronger southward tilt of the heliospheric current sheet for the rising phase of Solar Cycle 24, i.e., the "bashful ballerina" is responsible for asymmetric background solar wind conditions. The increase of the number of wave occurrences may be explained by a significant increase in the relative density of planetary protons with respect to the solar wind background. An exceptionally low solar wind proton density is observed during the rising phase of Solar Cycle 24. At the same time, higher EUV increases the ionization in the Venus exosphere, resulting in higher supply of energy from a higher number of newborn protons to the wave. We conclude that in addition to quasi- (anti)parallel conditions of the IMF and the solar wind velocity direction, the higher relative density of Venus exospheric protons with respect to the background solar wind proton density is the key parameter for the higher number of observable proton cyclotron waves near solar maximum.

1. Waves at the Ion Cyclotron Frequency in the Spacecraft Frame

In general, particle detectors provide a direct means to prove the existence of specific ions in the atmosphere of planets and satellites. In cases of a too low ion number density, detection may still be possible from the observation of their respective ion cyclotron waves in the local magnetic field data. This indirect detection method is especially useful in the upstream region of a planetary bow shock, in the outer atmosphere of planets or in the coma of comets. The observation of ion cyclotron waves from planetary particles in the interplanetary magnetic field (IMF) is the first sign of the approaching body.

Photoionization, electron impact ionization, and charge exchange are the main ionizing processes for planetary neutrals [*Zhang et al.*, 1993]. The newborn ions form an unstable secondary ion population in the solar wind, the interaction between both populations may lead to wave generation from different instabilities. It is important to realize that waves generated by newborn planetary ions upstream of the bow shock are characterized by their specific frequency ω_{sc} and polarization in the spacecraft frame

$$\omega_{sc} = \pm n\Omega_i$$

where $\Omega_i = q/m\, B_t$ denotes the ion gyrofrequency, with mass m and charge q of the ion, magnetic field strength B_t. Resonance occurs mainly for the fundamental mode $n = 1$, the negative sign indicates a possible reversion of the wave polarity in the spacecraft frame, with respect to the polarity in the solar wind frame [*Brinca*, 1991]. This equation is obtained under the conditions of negligible velocity of the planetary particle with respect to the planet and spacecraft, wave propagation parallel to the magnetic field **B**, and anomalous Doppler effect (for full derivation, see e.g., *Delva et al.* [2011] and references therein). This means that parallel propagating waves generated from newborn planetary ions will always be observed in the spacecraft frame

at the local ion gyrofrequency, regardless of the value of the angle α_{VB} between $\boldsymbol{V}_{SW}$ and $\boldsymbol{B}$, where $\boldsymbol{V}_{SW}$ denotes the solar wind velocity.

The specific frequency in the spacecraft frame enables a clear distinction of waves generated by planetary protons from those generated by solar wind protons reflected at the bow shock, which are observed at a much lower frequency [see e.g., *Shan et al.*, 2014]. Also, pickup ions can occur anywhere upstream, whereas reflected solar wind protons are limited to the foreshock region.

The angle α_{VB} between $\boldsymbol{V}_{SW}$ and $\boldsymbol{B}$ determines the mechanism for wave generation, via the growth rate of unstable modes. For quasi-parallel or antiparallel conditions of $\boldsymbol{V}_{SW}$ and $\boldsymbol{B}$, the newborn ions form a field-aligned beam of exospheric protons; the free energy is in the parallel drift velocity of the ions relative to the background plasma. Here the ion/ion resonant right-hand instability is dominant, and wave growth is fast [*Brinca*, 1991; *Gary*, 1991]. Due to the anomalous Doppler effect, the right-hand mode will be observed in the spacecraft frame at the local proton cyclotron frequency and with a left-hand polarization [*Tsurutani and Smith*, 1986]. This type of resonance was reported from observations at comets [*Lee*, 1989; *Brinca*, 1991; *Tsurutani*, 1991; *Mazelle and Neubauer*, 1993] but also at Venus [*Delva et al.*, 2011] and Mars [*Mazelle et al.*, 2004]. For perpendicular conditions of $\boldsymbol{V}_{SW}$ and $\boldsymbol{B}$, the newborn ions form a pure ring distribution in velocity space and the left-hand mode (in the plasma frame) is unstable, but with smaller wave growth [*Huddleston and Johnstone*, 1992]. Here the free energy in the ring acts as source for the ion cyclotron waves, e.g., at comets [see e.g., *Coates et al.*, 1990], at Mars [see e.g., *Bertucci et al.*, 2005], at Saturn [*Smith and Tsurutani*, 1983; *Leisner et al.*, 2006], and at Jupiter's satellites [e.g., *Huddleston et al.*, 1997; *Volwerk et al.*, 2001].

When intermediate values of the angle α_{VB} occur, a ring-beam distribution is formed in velocity space; with increasing values of α_{VB}, i.e., near $\alpha_{VB} = 70°$, a transition from one generation mechanism to the other will take place [*Gary*, 1991].

Upstream proton cyclotron waves were detected in the magnetometer data from Venus Express, showing that Venus (lacking an intrinsic magnetic field) is permanently losing hydrogen directly to the solar wind [*Delva et al.*, 2008a]. A statistical study for two Venus years at solar minimum conditions revealed the main properties of the waves [*Delva et al.*, 2008b]. Conditions favorable for cyclotron wave generation were found to be stable (anti)parallel configurations of $\boldsymbol{V}_{SW}$ and $\boldsymbol{B}$, which is in agreement with theory. Also, wave occurrences are independent of the direction of the motional electric field, indicating that they are generated from newborn protons of locally available hydrogen in the Venus exosphere [*Delva et al.*, 2011].

In the present study we analyze magnetometer [*Zhang et al.*, 2008] and Analyzer of Space Plasmas and Energetic Atoms (ASPERA)-plasma data [*Barabash et al.*, 2007; *Lundin*, 2011] from the Venus Express mission for two Venus years in the rising phase of Solar Cycle 24, for 450 days corresponding to 450 orbits from 1 March 2011 to 31 May 2012. The highest increase of solar activity was seen until 31 May 2012, with the highest sunspot number so far in May 2012. We study the specific wave properties and generation scenario under solar maximum conditions and compare with our earlier findings for solar minimum. The comparison leads to significant differences, and an attempt is made to explain these findings.

2. Data Analysis Method

Magnetic field data in the Venus Solar Orbital (VSO) reference frame with 1 Hz sampling rate are analyzed over a period of two full rotations of the spacecraft orbital plane about the polar axis of the planet, in order to provide equal data coverage for all planetary plasma regions. The solar wind velocity $\boldsymbol{V}_{SW}$ is taken to be radially outward from the Sun; the VSO reference frame is centered at Venus, with x_{VSO} axis positive toward the Sun and opposite to $\boldsymbol{V}_{SW}$, z_{VSO} axis perpendicular to Venus' orbital plane and positive to ecliptic north, and y_{VSO} axis completing the right-hand system. The magnetic field direction is described by the cone angle $\theta(-\boldsymbol{V}_{SW}, \boldsymbol{B})$ and the clock angle $\psi = \arctan(Bz_{VSO}/By_{VSO})$; B_{perp} denotes the $\boldsymbol{B}$ component perpendicular to $\boldsymbol{V}_{SW}$.

A static model for the Venus bow shock, as determined from the positions of observed bow shock crossings, was used [*Zhang et al.*, 2008]. Data from 20 min up to 4 h before and after the bow shock crossing were selected, and power spectra were calculated from 10 min data intervals. As for the wave study for solar minimum conditions (10 May 2006 to 10 August 2007) the proton cyclotron waves (PCWs) are identified in an automated
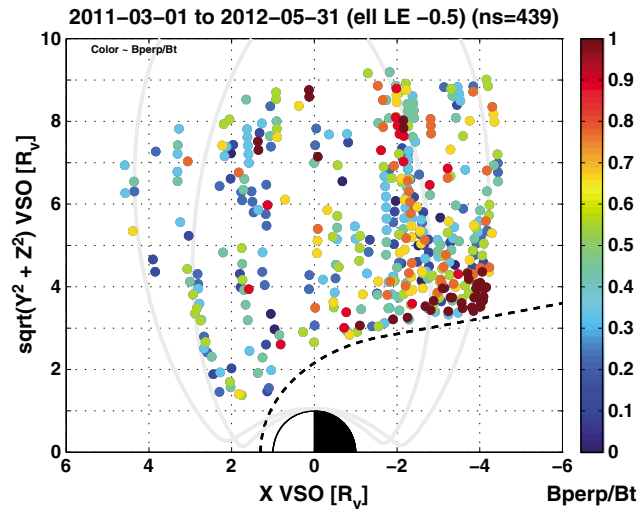
Figure 1. Positions of observations of PCWs from 1 March to 31 May 2012 in cylindrical VSO coordinates. Colors are according to B_{perp}/B_t; grey lines indicate approximately the limiting orbits of the spacecraft, regions outside of these lines were not accessed.

way from the power in a frequency interval $[0.8\,(f_p - \Delta f_p), f_p + \Delta f_p]$ near the local proton cyclotron frequency $f_p = (2\pi)^{-1}\,q/m\,B_t$ (see explanations in *Delva et al.* [2008b]). The following selection criteria are used

$$P_T/P_C > 1.5 \quad P_L/P_R > 1.5 \quad \text{ellipticity} < -0.5$$

where P_T and P_C denote the transverse and compressional component of the power spectrum, P_L and P_R the left-hand and right-hand polarized component of the transverse power in the spacecraft frame [*McPherron et al.*, 1972]; the inequality condition on the ellipticity ensures left-hand polarization in the spacecraft frame.

3. Observations Near Solar Maximum

3.1. General Properties

From the analysis of the data from 1 March 2011 to 31 May 2012 near solar maximum, a total number of 439 events of upstream PCW observations in single intervals of 10 min was found, up to a distance of 9 Venus radii (R_V) from the Venus-Sun line. With 439 cases of 10 min intervals there is an increase of occurrences by a factor of nearly 3, compared to only 153 events for solar minimum. The spatial distribution of these events in cylindrical VSO coordinates, shown in Figure 1, is very similar to the solar minimum case. The color coding in Figure 1, according to the relative perpendicular component B_{perp}/B_t of the field, clearly indicates that waves for quasi-perpendicular conditions (cone angle θ in (45°, 135°) or $B_{perp}/B_t > 0.7$) occur mainly downstream of the terminator plane. For such conditions of V_{SW} and $\boldsymbol{B}$, wave growth is slower and more newborn ions are needed; these waves become observable only after propagating through the region with the highest neutral density, which is in the terminator plane. Again, this is similar to the solar minimum case.

Table 1 lists the wave properties amplitude, ellipticity, and polarization for solar minimum [from *Delva et al.*, 2008b] and near solar maximum from the 10 min intervals; amplitude and ellipticity are comparable, but polarization is slightly higher near solar maximum.
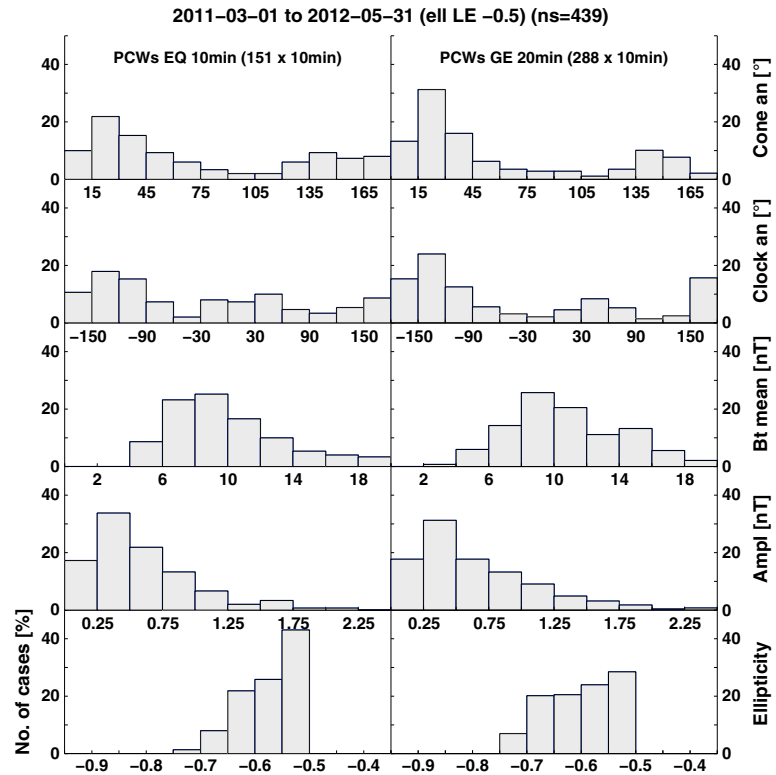
Table 1. Statistics of PCW Properties in 10 min Intervals

Wave Property	Median	First Quartile	Third Quartile
At Solar Minimum (ns = 153)			
B_t (nT)	9.88	7.52	11.92
Frequency (Hz)	0.15	0.11	0.18
Amplitude (nT)	0.56	0.32	0.82
Ellipticity	−0.61	−0.56	−0.67
Polarization (%)	63.40	55.33	72.49
Near Solar Maximum (ns = 439)			
B_t (nT)	9.99	8.07	12.77
Frequency (Hz)	0.16	0.12	0.19
Amplitude (nT)	0.50	0.31	0.85
Ellipticity	−0.59	−0.54	−0.64
Polarization (%)	75.92	68.40	83.41

Figure 2. Histograms (in %) for main parameters from 10 min PCW occurrence intervals, for (left) short wave occurrences (10 min, $ns = 151$) and for (right) longer-wave occurrences ($\geq$ 20 min, $ns = 285$ single intervals of 10 min).

When the 439 single events are grouped in trains of continual observations of 10 min intervals or longer we obtain a total of 254 sequences, with 156 occurrences of only 10 min duration and 98 wave occurrences lasting 20 min and longer. These are unexpected results: more and longer-wave occurrences are found near solar maximum, which indicates that in 38% of the cases (98 sequences out of 254) the spacecraft traveled through a large region of stable conditions for wave generation. For solar minimum conditions, only 25% of the PCW observations (26 out of 98) lasted over a time of 20 min or longer.

A more detailed investigation of the field conditions during the wave occurrences, separated into short- and long-duration observations, is shown in Figure 2. In agreement with theory and previous observational analysis at solar minimum, the PCWs are mainly observed for quasi- (anti)parallel conditions (top panel). However, now a clear asymmetry in the cone angles is seen: more waves occur under antiparallel conditions (cone angle $\theta < 45°$), and this is even more pronounced for the longer-lived waves ($\theta \leq 30°$). Smaller cone angles coincide with more clock angles ψ in $(-180°, -120°)$ and $(150°, 180°)$, which is consistent with antiparallel conditions. In general, the magnetic field strength $B_t \sim 8$–10 nT is slightly higher than for solar minimum (middle panel). Amplitudes are slightly larger, and ellipticities are more negative (i.e., the waves are more quasi-circular polarized) for the longer-wave occurrences (lower and bottom panel).

3.2. PCWs and Motional Electric Field

We study the distribution of the wave occurrence with respect to the direction of the electric field. This analysis is restricted to cases with well-defined cone angle in the range $(20°, 160°)$ to avoid the bias for badly defined direction of the electric field due to the data accuracy limit [± 1 nT], i.e., for small cone angles and low total field B_t. A Venus centered electromagnetic reference frame VBE is used with x_{VBE} axis positive toward the Sun, y_{VBE} axis positive in direction of the local mean magnetic field component perpendicular to Venus-Sun line, z_{VBE} axis positive in direction of motional electric field $\boldsymbol{E} = -\boldsymbol{V}_{SW} \times \boldsymbol{B}$. In this reference frame, the $\boldsymbol{B}$ field is in the (x_{VBE}, y_{VBE}) plane and the component perpendicular to $\boldsymbol{V}_{SW}$ is $B_{perp} = By_{VBE} \geq 0$; B_{perp} is proportional to the $\boldsymbol{E}$ field strength.
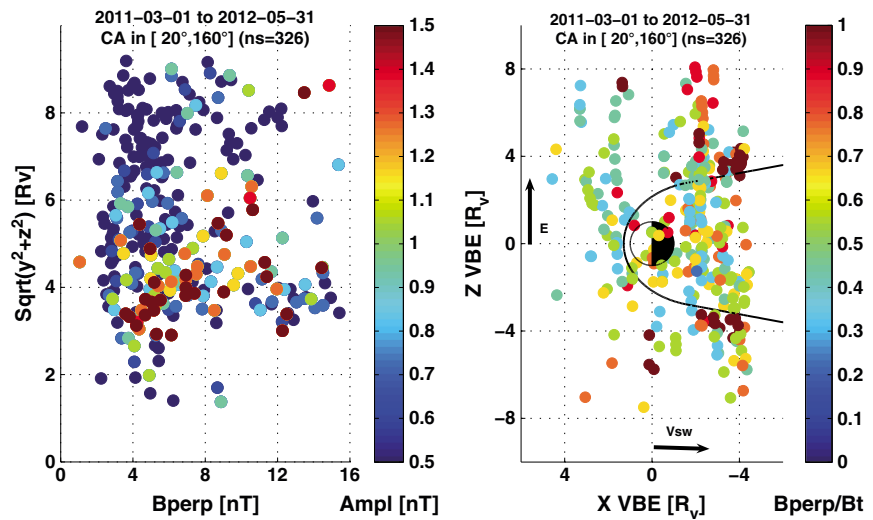
Figure 3. PCW observation positions as function of the perpendicular field component B_{perp}, restricted to cases with well-defined motional electric field, i.e., cone angle in (20°, 160°), $ns = 326$. (left) Distance to Venus-Sun line, color coding according to wave amplitude. Also for small but well-defined B_{perp} or weak electric field, waves are observed up to large distances. (right) In the VBE reference frame, color coding according to B_{perp}/B_t which is proportional to the electric field strength; waves are observed far into regions of negative electric field and far in direction toward the Sun; the black line denotes the modeled bow shock.

The independence or dependence of the PCW occurrences on the direction and strength of the electric field is important to distinguish if wave generation occurs at initial or secondary ionization. Secondary ionization involves fast planetary neutrals, which after initial ionization were accelerated in direction of positive electric field and then reneutralized (e.g., by charge exchange). An extensive discussion of the possibility of wave generation at secondary ionization was given in the study for solar minimum; there the occurrence of PCWs was found to be independent from the direction of the motional field, giving evidence that wave generation takes places at initial ionization from locally available planetary hydrogen.

Figure 3, left (color coding according to wave amplitude) shows the distance of the positions of PCW observations to the Venus-Sun line as function of B_{perp}. Waves occur at small and large distances for all values of B_{perp}, this means that pickup of planetary protons is not dependent on the strength of the motional electric field. Figure 3, right (color coding according to B_{perp}/B_t) shows the positions in the (x_{VBE}, z_{VBE}) plane; positions are found in both directions of the electric field. Since PCWs are propagating nearly parallel to $\boldsymbol{B}$, in this figure they will travel from left to right on lines parallel to the x_{VBE} axis, because the projection of any magnetic field line to the (x_{VBE}, z_{VBE}) plane is parallel to the x_{VBE} axis. Therefore, the waves have to be generated on that line further upstream than the observed position. This occurs in the negative as well as in the positive $\boldsymbol{E}$ hemisphere, indicating that the waves are generated at initial ionization of planetary hydrogen, sufficiently available in a large volume of space upstream of the planet. The panel also shows that under quasi-perpendicular conditions (cone angle θ in (45°, 135°) or $B_{perp}/B_t > 0.7$), PCWs occur mainly downstream of the terminator plane. Since under quasi-perpendicular conditions more newborn ions are required for a wave to grow to observable amplitude [*Cowee et al.*, 2012], this will be the case after passing through the region of highest local hydrogen density, which is in the terminator plane.

4. Solar Wind and PCWs at Solar Minimum and Maximum

4.1. Solar Wind Magnetic Field Conditions at Venus

The analysis in the previous section shows that now more longer-lived wave sequences are observed. This was not expected, since the IMF direction is generally less stable for solar maximum, and cone angle stability was found to be a condition for PCW generation [*Delva et al.*, 2011]. Therefore, we check the stability of the IMF cone angles in the undisturbed solar wind, in cone angle bins of 30° width. Figure 4 shows the number of cases per bin, where the cone angle remains within the bin for a duration of 10 to 100 min, Figure 4 (top) for solar
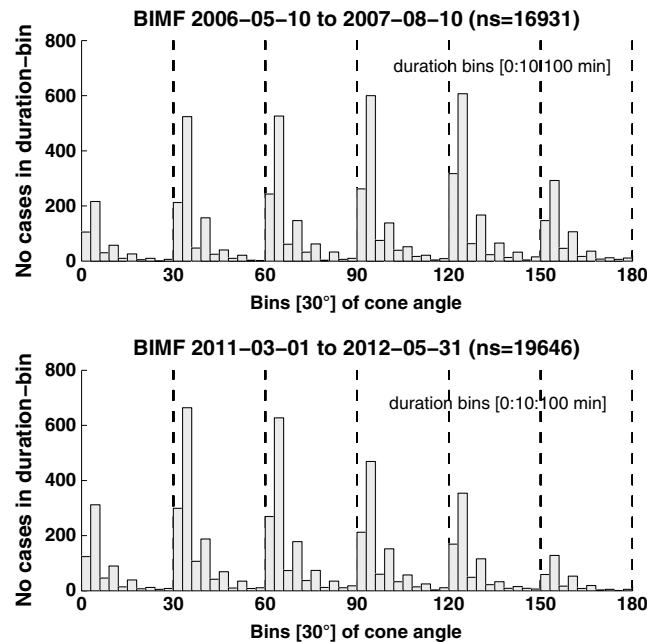
Figure 4. Stability of the IMF cone angles in the unshocked solar wind at Venus, for (top) solar minimum and (bottom) near solar maximum. The histograms show the number of cases where the cone angle remains in a cone angle bin (bin size 30°) for a duration of 10 to 100 min.

minimum, Figure 4 (bottom) near solar maximum. In both cases, the cone angle is mainly stable within a 30° interval for a duration of 20 min, and also 40 min or longer is possible. For solar minimum, the stable cases are almost equally spread over antiparallel and parallel conditions, whereas for solar maximum these occur preferably for antiparallel conditions (cone angles in (0°, 60°)). This proves that the stability of the field directional conditions in both cases is comparable; therefore, a change in stability cannot be the reason for the enhanced occurrence of longer-lived wave trains near solar maximum.

Furthermore, the occurrence of PCWs is significantly higher near solar maximum (by a factor of 3 compared to solar minimum), and the waves are mainly observed for antiparallel conditions of B and V_{SW} (Figure 2). However, the theoretical approach of the ion/ion beam resonance mechanism predicts no difference between parallel and antiparallel field directions [*Gary et al.*, 1993]. In addition, given the long time interval of two Venus years, an equal distribution of positive and negative field sectors in the solar wind would be expected. In order to detect an eventual asymmetry in the solar wind itself, we perform a more detailed analysis of the overall IMF conditions for solar minimum and near solar maximum.

The magnetic field in the unshocked solar wind is investigated in subintervals of 10 min, for times from 10 min (20 min near solar maximum) up to 4 h upstream of the model bow shock. Figure 5 shows the B direction and components relative to V_{SW} for solar minimum (left column) and near solar maximum (right column). The first panels display the distribution of the cone angles: in the left column for solar minimum, the rate of occurrence of quasi-parallel ($\theta > 135°$) and quasi-antiparallel ($\theta < 45°$) conditions is nearly equal, with slightly more parallel conditions; for solar maximum, a strong asymmetry is seen and the antiparallel conditions ($\theta < 45°$) prevail. Near solar maximum stronger fields occur (third panel); positive parallel components toward the Sun prevail and some larger values of the perpendicular component occur than for solar minimum (fourth and fifth panels, respectively). This proves that the IMF in the undisturbed solar wind is asymmetric near this solar maximum.

4.2. Solar Wind Plasma Conditions at Venus

From the ASPERA instrument [*Barabash et al.*, 2007; *Lundin*, 2011] solar wind total velocity and proton density data are now available on a long-time base, which we analyze for both time intervals. However, velocity direction data are not available for these long time intervals; therefore, V_{SW} is assumed to be radially outward from the Sun. The solar wind speed data upstream of the bow shock are averaged to one value per day. The histograms of V_{SW} in Figure 6 (blue lines; solar minimum left, near solar maximum right) show that V_{SW} is about 100 km s^{-1} higher near solar maximum. In addition, we check the solar wind speed for days with PCW occurrence; the red lines in Figure 6 display histograms of the relative occurrence of PCWs as function of V_{SW}. It can be seen that in solar minimum, the PCWs occur mainly for lower to normal V_{SW} (200–400 km s^{-1}); near solar maximum, waves occur for somewhat higher values (300–400 km s^{-1}). This fits with the generally higher speed near solar maximum; however, there are only few wave occurrences for V_{SW} higher than 400 km s^{-1}.

We conclude that independent of the level of solar activity, PCWs are mainly observed for slow to mean solar wind speeds of 200–400 km s^{-1}. From theory and numerical simulations, it was shown that the growth rate
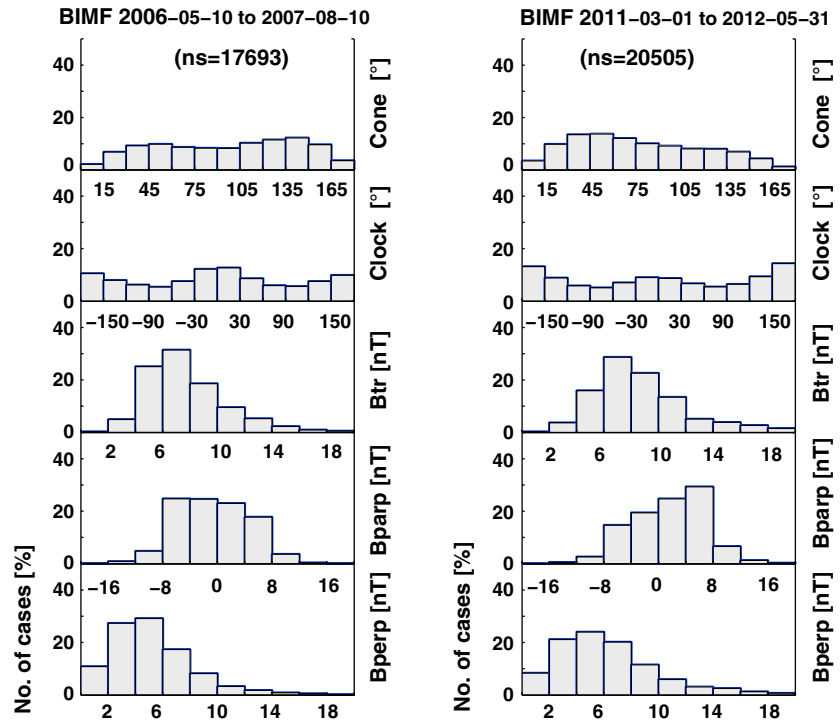
Figure 5. General properties of the IMF in the unshocked solar wind at Venus, for (left) solar minimum and (right) near solar maximum. For solar minimum, the rate of occurrence of quasi-parallel (cone angle $\theta > 135°$) or quasi-antiparallel ($\theta < 45°$) conditions is nearly equal, with slightly more parallel conditions. Near solar maximum a strong asymmetry is seen, the quasi-antiparallel conditions ($\theta < 45°$) prevail.

of the waves decreases with decreasing relative velocity of the beam with respect to the background plasma [*Gary et al.*, 1986]. The PCW observations are not in agreement with this prediction; this may be connected to the limited space with available newborn ions. Supply of newborn ions to the instability is limited to the relatively small volume of the Venus upper atmosphere. For low V_{SW} a longer time is needed to cross that region, and more newborn ions can contribute with their energy to the growing instability. Therefore, it may be possible that also for low solar wind speed the wave growth rate is sufficiently large to create the observed waves.

The density is another important parameter of the solar wind. The proton number densities as measured by ASPERA [*Lundin*, 2011] are somewhat biased: at specific times in the orbit, the instrument is in the shadow
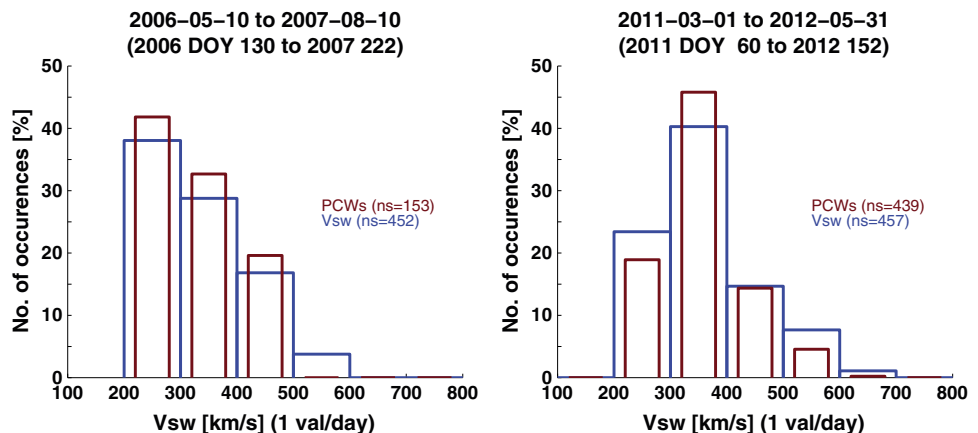

Figure 6. Histogram (in %) of observed solar wind speed (ASPERA, blue) and of 10 min PCW intervals (MAG, red) as function of the observed solar wind speed, for (left) solar minimum and (right) near solar maximum.
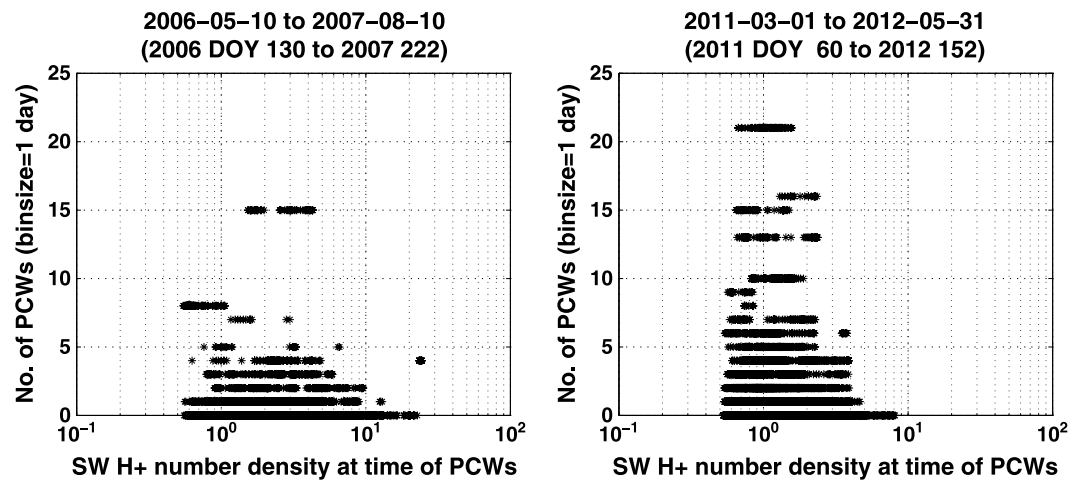
Figure 7. Observed number of PCW (10 min) intervals per day, as function of the solar wind proton number density (ASPERA), for (left) solar minimum and (right) near solar maximum. A general tendency of more PCWs for lower solar wind density is seen in both cases.

of some spacecraft parts, such that a too low density may be obtained. In general, the measured solar wind proton number density n_p is in the range 1–$10\,\text{cm}^{-3}$, where a true value of $n_p \sim 15\,\text{cm}^{-3}$ is expected. Therefore, daily averages of the solar wind proton density may be misleading, and we here use the full measured unaveraged data for the times of interest. Even if densities are underestimated, it will be in the same manner for solar minimum and maximum. Figure 7 shows the number of wave occurrences (in 10 min intervals) per day, as function of the ASPERA solar wind proton density for these times. For solar minimum (Figure 7, left), for days without PCWs, n_p ranges from 0.5 to 20 cm^{-3}; higher numbers of PCWs occur only for densities lower than ~5 cm^{-3}. Near solar maximum (Figure 7, right), the overall solar wind proton number density for times without PCWs is changed by a factor 0.5, from 0.5 to 8 cm^{-3}; the trend for more PCWs for lower densities ($n_p < 3$ cm^{-3}) is also clearly visible.

This leads to the conclusion that PCWs occur preferably for lower background solar wind density, which means that the relative density of the newborn planetary protons with respect to the background solar wind protons plays a significant role. Since the measured solar wind proton density here is generally lower for solar maximum (change by a factor 0.5), the higher number of PCW occurrences is in agreement with this result.

4.3. Exceptional Solar Wind Conditions During Solar Cycle 24

The findings of an asymmetrical sector distribution in the IMF at Venus during two Venus years near solar maximum, with more IMF in direction to the Sun, are unexpected. The significantly lower solar wind proton density for only slightly enhanced solar wind speed is also not in accordance with the known rules for the ascending solar activity branch near maximum. We therefore survey the specific solar wind properties for the decline of Solar Cycle 23 (2006–2007) and current Solar Cycle 24 (from January 2008 until latest data in early 2013).

In recent years, the concept of the "bashful ballerina" was put forward by several authors. Long-term observations (from ~1974 to date) in the ecliptic plane, as well as out of ecliptic by Ulysses, found a significant asymmetry in the sector distribution of the IMF during each solar cycle [e.g., *Smith et al.*, 2000; *Mursula and Hiltula*, 2003; *Mursula and Virtanen*, 2012; *McComas et al.*, 2013]. This is explained by a southward tilt of the heliospheric current sheet, such that the northern solar hemisphere has a larger extent than the southern one (see e.g., Figure 6 in *Smith et al.* [2000]). As a consequence, any spacecraft near the ecliptic plane will spend more time in the northern hemisphere and merely observe its specific polarity of the respective solar cycle. At the end of Solar Cycle 23 (2005–2007) a slight dominance of outward IMF was observed; for Solar Cycle 24, the IMF direction in the northern solar hemisphere is mainly toward the Sun (Figure 8, from *Mursula and Virtanen*, 2012, Figure 3 bottom panel).

This observation exactly fits with the findings from Venus Express, with its orbit approximately in the ecliptic plane. During the two Venus years in solar minimum (10 May 2006 to 10 August 2007) a slight
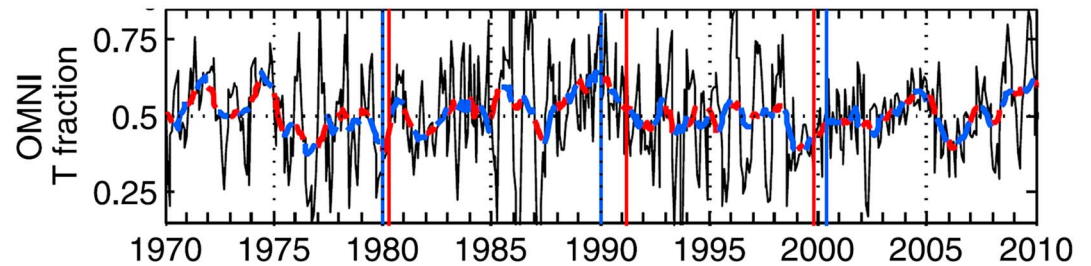
Figure 8. T-sector occurrence ratios T(T + A) for Pioneer 10 and 11, Voyager 1 and 2, and OMNI data. Thin line: 27 day averages; thick-colored line: 13 rotation running means stepped every 27 days. Blue (red) color indicates that the probe was above (below) equator. Vertical blue (red) lines mark the northern (southern) polar field reversal times according to Wilcox Solar Observatory [from *Mursula and Virtanen*, 2012, Figure 3 (bottom)].

prevalence of outward IMF was found (Figure 5, left). For the two Venus years near solar maximum (1 March 2011 to 31 May 2012) the prevalence of inward IMF is very clear (Figure 5, right). The observation of more PCW occurrences for quasi-antiparallel B and V_{SW} is therefore solely due to the tilt of the heliospheric current sheet in the current phase of Solar Cycle 24 and northern solar hemisphere with inward field.

The maximum of the present solar cycle is also exceptional in its sunspot number and solar wind density; a recent study by *McComas et al.* [2013] speaks of the "weakest solar wind of the space age and the current 'mini' solar maximum." For Solar Cycles 21 to 24 since 1974, a clear correlation was found between the monthly sunspot number and the tilt of the heliospheric current sheet (Figure 4f in *McComas et al.* [2013]). However, a deviation started from around the year 2000 up to date, such that the sunspot number increases only very weakly with the observed tilt increase; the lack of sunspots is most severe in 2013 (data considered up to 2013 day of year 79). A similar deviation is found in the solar wind proton density in the ecliptic plane: the H^+ density in 2008–2013 is only half of the value in 2005 (Figure 4c therein) and therefore extremely low. Also, this observation is in agreement with the observed solar wind proton density from Venus Express.

4.4. Effect of EUV on Venus Hydrogen Exosphere

Hybrid numerical simulations showed that a planetary ion density as low as ~0.01% of the solar wind density is sufficient to produce observable ion cyclotron waves [*Cowee et al.*, 2012]; also, continual supply of newborn ions under constant field conditions leads to faster wave growth and longer survival of the waves [*Cowee et al.*, 2008]. For solar minimum, the observation of the upstream PCWs proved that the ratio of the planetary proton density to the background solar wind proton density at Venus is high enough to support wave growth to observable amplitudes, preferably under stable (anti)parallel conditions [*Delva et al.*, 2011].

This poses the question, what is that ratio near solar maximum? For the investigated time interval, the EUV photon flux is a factor 1.5–2 higher than for solar minimum (data courtesy of SOHO-SEM, http://www.usc.edu/dept/space_science/semdatafolder/) and the ionization rate in the Venus exosphere will be increased as well. This is expected to have a nonnegligible effect on the number density of newborn protons in the exosphere.

Models for the thermosphere of Venus calculate the number density of cold hydrogen, up to an altitude of 400 km, for different solar activity, and predict a lower cold hydrogen density for solar maximum with only 20% of the value at solar minimum [*Fox and Sung*, 2001]. On the basis of these thermospheric results, *Lichtenegger et al.* [2013] modeled the hot hydrogen corona and the planetary H^+ density up to an altitude of 60 000 km (~10 R_V). Although starting from a lower hydrogen thermospheric density for solar maximum, the higher solar EUV leads to an increased ionization rate of the hot hydrogen. This results in a somewhat higher number density for H^+; at higher altitudes the increase is about 40% compared to solar minimum.

The measured lower density (change by a factor 0.5) of the solar wind protons in 2008–2013 [*McComas et al.*, 2013], also found in the ASPERA data, and the modeled higher density of exospheric protons (increase by a factor 1.4) for high solar activity lead to an expected enhancement of the density ratio of planetary protons relative to the solar wind background by a factor 2 to 3. A higher number of newborn planetary ions supply more energy to the growing waves, leading to a higher occurrence rate of PCWs near solar maximum. This also explains the longer-lived waves, because relatively more newborn ions allow faster wave growth and earlier detection of the waves in the data.

5. Conclusions

We have studied the occurrence of upstream proton cyclotron waves at Venus from magnetometer data of the Venus Express spacecraft for two Venus years (1 March 2011 to 31 May 2012) near solar maximum in the current Solar Cycle 24. We found an increase of the wave occurrences by a factor 3. The magnetic field conditions are similar to earlier findings at solar minimum and in general, the waves occur under quasi- (anti)parallel configurations of the magnetic field direction and the solar wind velocity. This is in accordance with theory, which predicts wave growth to observable amplitudes from the ion/ion beam resonance at (anti)parallel injection of newborn planetary ions into the background solar wind flow. However, an asymmetry in favor of more antiparallel conditions is found. Investigation of the magnetic field direction from the data in the unshocked solar wind shows the same tendency. Observations from other spacecraft reveal that the southward tilt of the heliospheric current sheet is responsible for a prevalence of the northern solar hemisphere with currently inward field during Solar Cycle 24. The asymmetry in the proton cyclotron wave occurrence can be explained by the "bashful ballerina" effect of the tilted heliospheric current sheet. The increase of the wave occurrence near solar maximum may be explained by a combination of several effects. The main cause is believed to be the increase of the ratio of the newborn planetary proton density to that of the background solar wind protons. The increased ratio is due to two different effects, which enforce each other. For high solar activity, the overall density of the solar wind is lower; this is especially the case for Solar Cycle 24, where an extremely low proton number density is measured. On the other hand, the number density of newborn ions in the Venus exosphere is expected to be higher due to the higher EUV flux in solar maximum. The two effects act as enhancement for the proton density ratio, leading to an increase in the growth of proton cyclotron waves to observable amplitudes. Furthermore, PCWs were mainly observed for low solar wind velocities ($< 400 \, \mathrm{km \, s^{-1}}$); this may be explained by the thus longer travel time of the wave through a limited space volume, allowing more newborn ions to interact with the wave. We conclude that in addition to stable quasi- (anti)parallel conditions of the IMF and the solar wind velocity direction, the relative density of the newborn exospheric ions with respect to the background solar wind density is a key parameter for upstream ion cyclotron wave generation.

References

Barabash, S., et al. (2007), The loss of ions from Venus through the plasma wake, *Nature*, *450*, 650–653, doi:10.1038/nature06434.

Bertucci, C., C. Mazelle, and M. Acuna (2005), Interaction of the solar wind with Mars from Mars Global Surveyor MAG/ER observations, *J. Atmos. Sol. Terr. Phys.*, *67*, 1797–1808.

Brinca, A. L. (1991), Cometary linear instabilities: From profusion to perspective, in *Cometary Plasma Processes*, *Geophys. Monogr. Ser.*, *61*, 211–221.

Coates, A. J., B. Wilken, A. D. Johnstone, K. Jockers, K. H. Glassmeier, and D. E. Huddleston (1990), Bulk properties and velocity distributions of water group ions at Comet Halley: Giotto measurements, *J. Geophys. Res.*, *95*, 10,249–10,260, doi:10.1029/JA095iA07p10249.

Cowee, M. M., C. T. Russell, and R. J. Strangeway (2008), One-dimensional hybrid simulations of planetary ion pickup: Effects of variable plasma and pickup conditions, *J. Geophys. Res.*, *113*, A08220, doi:10.1029/2008JA013066.

Cowee, M. M., S. P. Gary, and H. Y. Wei (2012), Pickup ions and ion cyclotron wave amplitudes upstream of Mars: First results from the 1D hybrid simulation, *Geophys. Res. Lett.*, *39*, L08104, doi:10.1029/2012GL051313.

Delva, M., T. L. Zhang, M. Volwerk, W. Magnes, C. T. Russell, and H. Y. Wei (2008a), First upstream proton cyclotron wave observations at Venus, *Geophys. Res. Lett.*, *35*, L03105, doi:10.1029/2007GL032594.

Delva, M., T. L. Zhang, M. Volwerk, Z. Vörös, and S. A. Pope (2008b), Proton cyclotron waves in the solar wind at Venus, *J. Geophys. Res.*, *113*, E00B06, doi:10.1029/2008JE003148.

Delva M., C. Mazelle, C. Bertucci, M. Volwerk, Z. Vörös, and T. L. Zhang (2011), Proton cyclotron wave generation mechanisms upstream of Venus, *J. Geophys. Res.*, *116*, A02318, doi:10.1029/2010JA015826.

Fox, J. L., and K. Y. Sung (2001), Solar activity variations of the Venus thermosphere/ionosphere, *J. Geophys. Res.*, *106*(A10), 21,305–21,335, doi:10.1029/2001JA000069.

Gary, P. (1991), Electromagnetic ion/ion instabilities and their consequences in space plasmas: A review, *Space Sci. Rev.*, *56*, 373.

Gary, P., C. Madland, D. Shriver, and D. Winske (1986), Computer simulations of electro-magnetic cool ion beam instabilities, *J. Geophys. Res.*, *91*, 4188–4200, doi:10.1029/JA091iA04p04188.

Gary, S. P., M. E. McKean, and D. Winske (1993), Ion cyclotron anisotropy instabilities in the magnetosheath: Theory and simulations, *J. Geophys. Res.*, *98*(A3), 3963–3971, doi:10.1029/92JA02585.

Huddleston, D. E., and A. D. Johnstone (1992), Relationship between wave energy and free energy from pick-up ions in the Comet Halley environment, *J. Geophys. Res.*, *97*, 12,217–12,230, doi:10.1029/92JA00726.

Huddleston, D. E., R. J. Strangeway, J. Warnecke, C. T. Russell, M. G. Kivelson, and F. Bagenal (1997), Ion cyclotron waves in the Io torus during the Galileo encounter: Warm plasma dispersion analysis, *Geophys. Res. Lett.*, *24*, 2143–2146, doi:10.1029/97GL01203.

Lee, M. (1989), Ultra-low frequency waves at comets, in *Plasma Waves and Instabilities at Comets and in Magnetospheres*, *Geophys. Monogr. Ser.*, vol. 53, edited by B. T. Tsurutani and H. Oya, pp. 13–29, AGU, Washington, D. C.

Leisner J. S., C. T. Russell, M. K. Dougherty, X. Blanco-Cano, R. J. Strangeway, and C. Bertucci (2006), Ion cyclotron waves in Saturn's E ring: Initial Cassini observations, *Geophys. Res. Lett. 33*, L11101, doi:10.1029/2005GL024875.

Lichtenegger, H., M. Delva, H. Gröller, and C. Bertucci (2013), The puzzling hydrogen corona at Venus, European Planetary Science Congress 2013, Abstract EPSC2013-627.

Lundin, R. (2011), Ion acceleration and outflow from Mars and Venus: An overview, *Space Sci. Rev.*, *162*, 309–334, doi:10.1007/s11214-011-9811-y.

Mazelle, C., and F. M. Neubauer (1993), Discrete wave packets at the proton cyclotron frequency at comet P/Halley, *Geophys. Res. Lett.*, *20*, 153–156, doi:10.1029/92GL02613.

Mazelle, C., et al. (2004), Bow shock and upstream phenomena at Mars, *Space Sci. Rev.*, *111*(1–2), 115–181.

McComas, D. J., N. Angold, H. A. Elliott, G. Livadiotis, N. A. Schwadron, R. M. Skoug, and C. W. Smith (2013), Weakest solar wind of the space age and the current "mini" solar maximum, *Astrophys. J.*, *779*, 2, doi:10.1088/0004-637X/779/1/2.

McPherron, R. L., C. T. Russell, and P. J. Coleman (1972), Fluctuating magnetic fields in the magnetosphere, II, ULF waves, *Space Sci. Rev.*, *13*, 411–454.

Mursula, K., and T. Hiltula (2003), Bashful ballerina: Southward shifted heliospheric current sheet, *Geophys. Res. Lett.*, *30*(22), 2135, doi:10.1029/2003GL018201.

Mursula, K., and I. I. Virtanen (2012), The wide skirt of the bashful ballerina: Hemispheric asymmetry of the heliospheric magnetic field in the inner and outer heliosphere, *J. Geophys. Res.*, *117*, A08104, doi:10.1029/2011JA017197.

Shan, L., Q. Lu, M. Wu, X. Gao, C. Huang, T. Zhang, and S. Wang (2014), Transmission of large-amplitude ULF waves through a quasi-parallel shock at Venus, *J. Geophys. Res. Space Physics*, *119*, 237–245, doi:10.1002/2013JA019396.

Smith, E. J., and B. T. Tsurutani (1983), Saturn's magnetosphere: Observations of ion cyclotron waves near the Dione *L* shell, *J. Geophys. Res.*, *88*, 7831–7836, doi:10.1029/0JGREA000088000A10007831000001.

Smith, E. J., J. R. Jokipii, J. Kóta, R. P. Lepping, and A. Szabo (2000), Evidence of a north-south asymmetry in the heliosphere associated with a southward displacement of the heliospheric current sheet, *Astrophys. J.*, *533*, 1084–1089.

Tsurutani, B. (1991), Comets: A laboratory for plasma waves and instabilities, in *Cometary Plasma Processes*, *Geophys. Monogr. Ser.*, vol. 61, edited by A. Johnstone, pp. 189–209, AGU, Washington, D. C.

Tsurutani, B. T., and E. J. Smith (1986), Hydromagnetic waves and instabilities associated with cometary pick-up: ICE observations, *Geophys. Res. Lett.*, *13*, 263–266, doi:10.1029/GL013i003p00263.

Volwerk, M., M. G. Kivelson, and K. K. Khurana (2001), Wave activity in Europa's wake: Implications for ion pickup, *J. Geophys. Res.*, *106*, 26,033–26,048, doi:10.1029/2000JA000347.

Zhang, M. H. G., J. G. Luhmann, A. F. Nagy, J. R. Spreiter, and S. S. Stahara (1993), Oxygen ionization rates at Mars and Venus—Relative contributions of impact ionization and charge exchange, *J. Geophys. Res.*, *98*(E2), 3311–3318, doi:10.1029/92JE02229.

Zhang, T. L., et al. (2008), Initial Venus Express magnetic field observations of the Venus bow shock location at solar minimum, *Planet. Space Sci.*, *56*, 785–789.